On finding the relevant dynamics for model based controlling walking robots

E. Garcia (egarcia@iai.csic.es), J.A. Galvez and P. Gonzalez de Santos
Instituto de Automatica Industrial. La Poveda, 28500 Madrid, Spain
Phone. +34-918711900 FAX. +34-918717050
Category (3)

Abstract. Leg dynamics are often ignored in the real-time control of walking robots because of the high gearing used in leg transmissions. However, the use of a gear reduction high enough to discount Coriolis and centripetal components yields additional non-desired dynamics, which are friction, backlash and elasticity. In such cases, simplifying robot dynamics without considering the effect of gear dynamics leads to unavoidable errors. In order to make dynamic equations reflect the reality of the physical system, it is of paramount importance to model the most significant effects acting on the system. Robot dynamics could then be analyzed and related to trajectory parameters for motion-control purposes. In this paper, a method to derive the dynamics of a robot leg as a function of leg-trajectory parameters is proposed. The method experimentally finds the simplified equations of motion that reflect the reality of the physical system. The resulting model is an accurate and simple representation of the system dynamics, taking into account the most relevant dynamics affecting the system. The simplification of the model allows it to be used in a real-time dynamic-control system.

Keywords: Walking robots, robot dynamics, dynamic modeling, model-based control

1. Introduction

Walking robots are very complex mechanical systems, featuring a variable structure defined by its number of degrees of freedom (DOF). For designing algorithms for the control of walking robots it is important to have good models describing the dynamic behaviour of the robot. Nevertheless, obtaining a walking robot's equations of motion is extremely time-consuming and yields an indeterminate system of equations, which must be solved using some optimization criterion, e.g. optimal force distribution, employing the Lagrange-multipliers method [2, 14]. To simplify the problem, dynamic models of walking robots do not usually consider the dynamics of the legs, based on the assumption of high gearing and massless legs. However, this assumption should be ensured by means of a dynamic analysis of the robot to avoid errors due to an unreasonable simplification. In order to make dynamic equations reflect the reality of the physical system, it is important

to model the most significant effects acting on the system. A trade-off has to be established between an accurate model of the system and the viability of its real-time implementation for dynamic control. Therefore, robot-dynamics analyzing methods are needed that permit the simplification of the equations of motion without yielding significant errors during real-time control. As equations of motion are normally used for trajectory generation and control, the analysis should reflect which dynamic effects arise during the different robot movements.

Methods already exist for experimental identification of robot dynamics for model generation [1, 10, 18]. The equations of motion are derived through an experimental parameter-identification process based on a initial guess in the dynamic response of the system. However, the correctness of the initial guess is critical, and these methods do not give any insight into the conceptual and physical understanding of robot dynamics. In this paper, we propose a method for experimental dynamic analysis of a walking robot depending on trajectory parameters. The envisaged application is model-based robot control, e.g. computed torque control. The accuracy of these controllers relies highly on the ability of the model to accurately predict the required actuator torques. Therefore, the proposed method ascertains the main dynamic components affecting the system during different real leg trajectories, including actuator dynamics and friction. The mathematical model thus obtained results in an accurate simplified representation of system dynamics. The method is applied to the SILO4 quadruped robot, yielding a simple and at the same time accurate mathematical model which can be used by a real-time model-based control system.

The paper is structured as follows: First the dynamic equations for the leg are obtained in Section 2, taking actuator dynamics into account. Then a model analysis method is proposed as a function of trajectory parameters in Section 3. An application to the SILO4 quadruped robot is detailed in Section 4, and finally, relevant conclusions are found in Section 5.

2. Dynamic model

Robot dynamics state the relationship between robot motion and the forces involved therein. Specifically, the dynamic model of a robot manipulator finds mathematical relationships among:

1. Robot location and its derivatives, velocity and acceleration.
2. Forces and torques applied at the robot joints or end-effector.

3. Dimensional parameters of the robot manipulator, such as link length, mass and inertia.

Walking robots are very complex mechanical systems. The legs of a walking robot are connected to one another through the body and also through the ground, forming closed kinematic chains. Forces and moments propagate through the kinematic chain from one leg to another, and therefore dynamic coupling exists. The equations of motion of such a complex system with m legs each of n DOF are derived from d'Alembert's principle and are given in equation (1), where $\tau \epsilon \mathbf{R}^{n \times m}$ is the vector of active joint torques, $\mathbf{F} \epsilon \mathbf{R}^{m \times 3}$ is the vector of ground-contact forces, $\mathbf{D} \epsilon \mathbf{R}^{n \times m+6, n \times m+6}$ denotes the mass matrix, $\mathbf{q} \epsilon \mathbf{R}^{n \times m+6}$ is the vector of generalized coordinates, $\mathbf{H} \epsilon \mathbf{R}^{n \times m+6}$ denotes Coriolis and centrifugal effects, $\mathbf{C} \epsilon \mathbf{R}^{n \times m+6}$ denotes the generalized influence of gravitation, and $\mathbf{J}_M \epsilon \mathbf{R}^{n \times m, n \times m+6}$ and $\mathbf{J}_F \epsilon \mathbf{R}^{n \times m, n \times m+6}$ project the torques and contact forces, respectively, to the space of the generalized coordinates $\mathbf{q}$.

$$\mathbf{J}_M^T \tau - \mathbf{J}_F^T \mathbf{F} = \mathbf{D}(\mathbf{q})\ddot{\mathbf{q}} + \mathbf{H}(\mathbf{q}, \dot{\mathbf{q}}) + \mathbf{C}(\mathbf{q}) \tag{1}$$

Computing the above equations of motion is extremely time-consuming and yields a system of $2 \times n \times m$ unknown variables (τ and $\mathbf{F}$) with $n \times m + 6$ equations, which must be solved using some optimization criterion, e.g. optimal force distribution, employing the Lagrange-multipliers method [2, 14]. To simplify the problem, some assumptions are usually made based on the property of the robots' legs, which are high-geared robotic systems. Using high reduction ratios in the joints of the legs makes it possible to neglect the coupling effect of Coriolis and centrifugal forces and therefore to decouple the dynamic equations (1). However, high-geared mechanisms feature other specific dynamics, such as friction, backlash and elasticity [7, 13, 16, 17]. Therefore, if high reduction ratios are used in the robot joints, the dynamic equations can be decoupled, but other dynamic effects must be modeled instead.

A robotic leg can be studied from the dynamics point of view as a 3-DOF manipulator with a foot as end-effector. The dynamic model of a manipulator consists of the model of the mechanical part and the model of its actuators and transmission systems. The dynamic model of the mechanical part states the mathematical relationships between manipulator motion and the forces and torques causing it. On the other hand, the dynamic model of actuators and transmission systems finds relationships between control signals and forces and torques required for motion. We will derive the dynamic model of the actuators and

the mechanical part of the legs of a walking robot separately in the following subsections.

2.1. Dynamic model of the mechanical part

The mechanical part of a 3-DOF leg is the chain of serial links that conform the leg, excluding actuators and transmission systems. For deriving the dynamic equations of the mechanical part of the leg, the Lagrange-Euler formulation has been chosen [5]. The direct application of the lagrangian dynamics formulation together with the Denavit-Hartenberg link-coordinate representation results in a convenient, compact, systematic algorithmic description of the leg equations of motion. Although real-time computation of the Newton-Euler formulation [5] is still more efficient than the Lagrange-Euler equations in open-loop control, the fact is that today's processors are fast enough to compute efficiently the 4 x 4 homogeneous transformation matrices of the lagrangian formulation. The Lagrange-Euler formulation is a simple, secure method for deriving the mathematical expressions. Later analysis of the dynamic model of the leg will result in simplifications that ensure the real-time computation of the final equations of motion.

Systematic derivation of the Lagrange-Euler equations yields a dynamic expression that can be written in the form:

$$\tau_{\mathbf{e}} - \mathbf{J}^T\mathbf{F} = \mathbf{D}(\mathbf{q})\ddot{\mathbf{q}} + \mathbf{H}(\mathbf{q}, \dot{\mathbf{q}}) + \mathbf{C}(\mathbf{q}) \tag{2}$$

where $\mathbf{D}(\mathbf{q})$ is the 3×3 mass matrix of the leg, $\mathbf{H}$ is a 3×1 vector of centrifugal and Coriolis terms, and $\mathbf{C}(\mathbf{q})$ is a 3×1 vector of gravity terms.

The mass matrix is symmetric, positive-defined, and configuration-dependent. Its diagonal elements d_{ii} are the inertia moments of the mechanical part around joint i when all the rest of the joints are blocked. The d_{ij} elements represent the effect of the acceleration of joint j on joint i.

The vector of centrifugal and Coriolis terms is configuration-dependent and rate-dependent. Its h_i elements are the sum of quadratic terms in joint speed and represent the effects induced on joint i due to the speed of the rest of the joints.

Lastly, the vector of gravity terms is configuration-dependent. The c_i terms show the moments around joint i caused by gravity.

The first term in (2) consists of torques and forces required for trajectory tracking, where τ_e is the 3×1 vector of active joint torques and $\mathbf{F}$ is the 3×1 vector of ground-contact forces. During the leg-transfer phase, there is no foot/terrain interaction, and $\mathbf{F}$ becomes

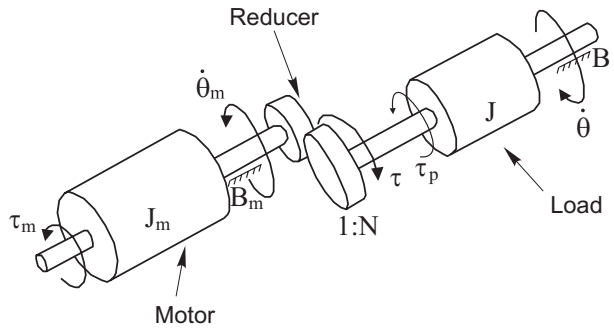

Figure 1. Mechanical model of a DC torque motor connected through gearing to an inertial load.

zero. However, during the support phase, ground contact exists, and (2) becomes undetermined and should be solved in one of these ways:

- Using Lagrange multipliers to minimize some energy function [4].
- Modeling foot/terrain interaction [9]. The relationship between contact forces and foot positions is established, therefore adding to the number of equations required to solve (2).
- Using force sensors at the feet to measure **F** [19].

2.2. Dynamic model of actuators and transmission systems

Actuators and transmission systems play a relevant role in the computation of robot dynamics. Actuators are mainly of three types, electric, pneumatic, and hydraulic. Electric actuators are more precisely controlled, however, and thus are more widely used. In the operation of DC motors, inertia and friction arise during rotor spin that must be balanced through the motor torque. Also, if high reduction gearing is used, as in walking robots, friction, elasticity and backlash are introduced.

In this paper only DC motors are considered, because they are the type of motor most usually found in the joints of legged robots. Dynamic models of hydraulic actuators can be found in [3, 15] while different models of pneumatic actuators are explained in [12]. Figure 1 shows the mechanical model of a DC torque motor connected through gear reduction to an inertial load. The torque applied to the rotor, τ_m, must balance both rotor and load inertias, which here we denote as

equivalent inertia, J_{eq}. Likewise it must balance damping effects due to motor and load friction, which we denote as equivalent damping, B_{eq}, that is:

$$\tau_m - \frac{1}{N}\tau_p = J_{eq}\ddot{\theta}_m + B_{eq}\dot{\theta}_m \tag{3}$$

where θ_m are actuator positions and N is the reduction coefficient. The equivalent inertia and damping are obtained from:

$$J_{eq} = J_m + \frac{1}{N^2}J \tag{4}$$

$$B_{eq} = B_m + \frac{1}{N^2}B \tag{5}$$

Transmission systems are another source of friction. Viscous friction is usually present in lubricated contacts; therefore this friction should be included in the equivalent damping term, B_{eq}. However, other friction components, like Coulomb friction, can also exist. This friction component is responsible for energy losses in the transmission and can be modeled using the mechanical efficiency of the reducer, η. Therefore, Coulomb and viscous friction in the transmission system can be included in the dynamic model as follows:

$$J_{eq} = J_m + \frac{1}{N^2\eta}J \tag{6}$$

$$B_{eq} = B_m + \frac{1}{N^2\eta}B \tag{7}$$

Nevertheless, this model transmission-system friction might not be precise enough for every system. The model considers neither static friction nor meshing friction [7], which is especially dominant in high-geared systems. In such cases, a friction model is required. A complete friction model for high-geared robotic systems can be found in [7].

2.3. The complete dynamic model

The dynamic model of the leg consists of the dynamic model of the mechanical part and the dynamic model of the actuators and transmission systems. Considering the mechanical part of the leg as a configuration-dependent load that the actuator torque must balance, the active actuator torques needed to move the mechanical part are taken from (2):

$$\tau_{\mathbf{a}} = \mathbf{N}^{-1}\tau_{\mathbf{e}} \tag{8}$$

where $\mathbf{N}$ is a 3×3 diagonal matrix of joint-reduction ratios. Actuator position, velocity and acceleration are related to joint position, velocity and acceleration:

$$\theta_{\mathbf{m}} = \mathbf{N}\mathbf{q}\,; \quad \dot{\theta}_{\mathbf{m}} = \mathbf{N}\dot{\mathbf{q}}\,; \quad \ddot{\theta}_{\mathbf{m}} = \mathbf{N}\ddot{\mathbf{q}} \tag{9}$$

where $\theta_{\mathbf{m}}$, $\dot{\theta}_{\mathbf{m}}$, and $\ddot{\theta}_{\mathbf{m}}$ are actuator position, velocity, and acceleration respectively, and $\mathbf{q}$, $\dot{\mathbf{q}}$, and $\ddot{\mathbf{q}}$ are joint position, velocity, and acceleration respectively.

The mass matrix $\mathbf{D}$ can be written as the addition of two matrices:

$$\mathbf{D}(\mathbf{q}) = \mathbf{D}_1 + \mathbf{D}_2(\mathbf{q}) \tag{10}$$

where $\mathbf{D}_1$ is the 3×3 diagonal matrix of the constant terms in $\mathbf{D}(\mathbf{q})$. Substituting (2), (9) and (10) in (8):

$$\tau_{\mathbf{a}} = \mathbf{N}^{-1}\mathbf{D}_1\mathbf{N}^{-1}\ddot{\theta}_{\mathbf{m}} + \tau_{\mathbf{p}} \tag{11}$$

where

$$\tau_{\mathbf{p}} = \mathbf{N}^{-1}\mathbf{D}_2(\theta_{\mathbf{m}})\mathbf{N}^{-1}\ddot{\theta}_{\mathbf{m}} + \mathbf{N}^{-1}\mathbf{H}(\theta_{\mathbf{m}}, \dot{\theta}_{\mathbf{m}}) + \mathbf{N}^{-1}\mathbf{C}(\theta_{\mathbf{m}}) + \mathbf{N}^{-1}\mathbf{J}^T\mathbf{F} \tag{12}$$

Thus, the dynamics of the mechanical part of the leg can be considered as the sum of two terms: a constant inertia given by $\mathbf{J} = \mathbf{N}^{-1}\mathbf{D}_1\mathbf{N}^{-1}$ and a perturbation $\tau_{\mathbf{p}}$ given by the variable terms in (2). Considering that the actuator torque must balance the leg dynamics, the dynamic model of the actuators can be expressed in a matrix form:

$$\tau_{\mathbf{m}} = \mathbf{J}_{\mathbf{eq}}\ddot{\theta}_{\mathbf{m}} + \mathbf{B}_{\mathbf{eq}}\dot{\theta}_{\mathbf{m}} + \tau_{\mathbf{p}} + \tau_{\mathbf{F}} \tag{13}$$

where $\tau_{\mathbf{m}}$ is a 3×1 vector of actuator torques. The equivalent inertia and damping are obtained from:

$$\mathbf{J}_{\mathbf{eq}} = \mathbf{J}_{\mathbf{m}} + \mathbf{N}^{-1}\mathbf{D}_1\mathbf{N}^{-1} \tag{14}$$

$$\mathbf{B}_{\mathbf{eq}} = \mathbf{B}_{\mathbf{m}} + \mathbf{F}_{\mathbf{v}} \tag{15}$$

where $\mathbf{J}_{\mathbf{m}}$ is a 3×3 diagonal matrix whose element $J_{m_{ii}}$ is the rotor inertia of actuator i. Likewise, $\mathbf{B}_{\mathbf{m}}$ is the 3×3 diagonal matrix whose element $B_{m_{ii}}$ is the coefficient of viscous friction of actuator i. $\mathbf{F}_{\mathbf{v}}$ is the 3×3 diagonal matrix whose element $F_{v_{ii}}$ is the coefficient of viscous friction in the transmission system of joint i. $\tau_{\mathbf{F}}$ is the 3×1 vector of the dynamic model of friction in each joint, excluding the viscous friction, $F_{v_{ii}}$.

Expressions (13), (14), (15) and (12) complete the dynamic model of a robot leg or manipulator. Notice that τ_p and τ_F are non-linear terms. Also the terms in τ_p are coupled between joints. Only if high reduction is used could this term be neglected and the model in (13), decoupled. However, in such cases the τ_F term will increase its relevance, and the model will become more complex. Therefore it is necessary to study and analyze the model to obtain a precise simplified expression.

3. A method for dynamic model analysis

The inherent complexity of the dynamic model of a robot leg or manipulator usually converges to an improper model simplification to enable real-time motion control. As a result, control will become imprecise due to a careless simplification procedure.

To enable an accurate simplification of the dynamic model, a method for dynamic analysis is here proposed consisting of four steps:

Step 1: Computation of each term in dynamic equation (13) during real robot trajectories covering the whole workspace.

Step 2: Analysis of the torque contribution of each computed term.

Step 3: If the torque contribution of a term in the model is less than 5% for every trajectory, then that term is considered non-significant and can be neglected.

Step 4: The remaining terms reflect the relevant dynamics. Then the evolution of these significant terms during different trajectories is studied as follows:

- Evolution of torque contributions as a function of end-effector position.
- Evolution of torque contributions as a function of linear-trajectory speed.
- Evolution of torque contributions as a function of linear-trajectory acceleration.

As a result of the analysis, the variation of the relevant robot dynamics during real robot tasks is identified. The relationship between robot dynamics and trajectory parameters can be used in a real-time control algorithm or in a maximum-speed trajectory generation algorithm [6].

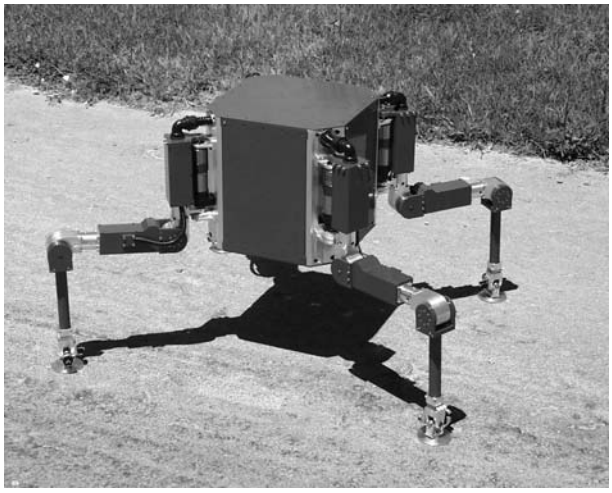

Figure 2. The SILO4 walking robot

4. Application to the SILO4 walking robot

The walking machine used in this work was designed as a small robot for education and basic research purposes. Although there are some legged robots in the market for research and education, they are basically toys with very low ground-adaptation capability and very weak mechanical construction. The main idea behind this new development is to configure a small, easy-to-handle, reliable walking robot with great terrain-adaptability features, to be used as a comparative test-bed of new methods and algorithms. The ground-adaptation capabilities of this robot require powerful limbs where dynamics cannot be neglected. Figure 2 is a picture of the SILO4 robot.

The leg of the SILO4 is based on an insect-like leg formed by slender links that contain the actuators. Each link is about 0.240 meters long, and the leg features an average speed of about 0.4 m/s (0.2 m/s when the foot follows a straight line). The leg is based on three rotary joints actuated by three DC motors with planetary and skew-axis gears. This leg has a special articulated three-passive-joint foot consisting of a universal joint (two passive joints) with a force sensor and a couple of potentiometers to measure joint orientation when the sole (another passive joint) is in its support phase. The position sensors help to find the components of the force acting on the foot.

Table I. Dynamic parameters of the SILO4 leg referred to Denavit-Hartenberg link coordinate representation.

Link parameter		Link 1	Link 2	Link 3 + foot
Mass (Kg)		1.22	1.26	0.63
Length (mm)		60.0	238.4	238.5
Position of the c.o.m. (mm)	x_{cm}	-12.2	-109.4	-84.5
	y_{cm}	101.0	11.4	-2.5
	z_{cm}	0.4	-0.8	3.9
Inertia tensor (10^{-3} Kg·m^2)	I_{xx}	18.2	0.6	0.3
	I_{xy}	1.7	1.8	-0.01
	I_{xz}	0.002	-0.17	0.17
	I_{yy}	0.6	22.4	10.8
	I_{yz}	-0.03	0.01	0.0
	I_{zz}	18.4	22.5	10.8

4.1. Dynamic model of the mechanical part

The Lagrange-Euler formulation was used to derive the dynamic equations of the mechanical part of the SILO4 leg. Direct application of the lagrangian dynamics formulation together with the Denavit-Hartenberg link coordinate representation resulted in a convenient, compact, systematic algorithmic description of the SILO4 leg's equations of motion. Table 1 lists all the dynamic parameters of the SILO4 leg used for the derivation of the dynamic equations of motion. Accurate values of inertial moments and centre-of-mass positions were computed using Pro/ENGINEER mechanical design software [8]. Mass values were checked experimentally.

Systematic derivation of the Lagrange-Euler equations yielded dynamic equation (2) for the mechanical part of the leg. Matrices D, H and C for the SILO4 leg can be found in Appendix B. The Maple V software package was used for symbolic simplification of the results [11].

4.2. Dynamic model of the actuators

The actuators of the SILO4 leg are three low-inertia DC motors, located at each joint and connected through gear reduction to the load. The first joint actuator is connected through a planetary gear, joints 2 and 3, however, have a planetary gear plus a skew-axis gear (see Figure 3). Thus, the first joint-motor assembly will match the model in Figure 1, while the joint-motor assemblies of joints 2 and 3 have two gear stages and thus will have a more complex model. If we want to achieve

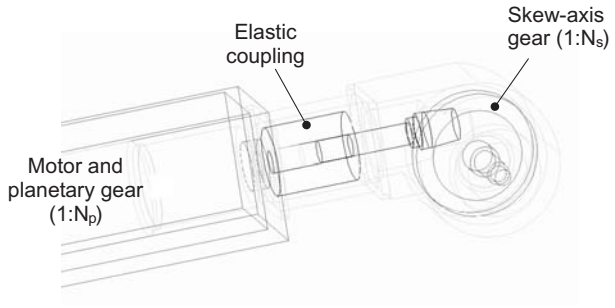

Figure 3. Transmission and gearing of 2nd and 3rd joints of the SILO4 leg

an accurate model of these actuators, we should bear in mind that they are non-ideal actuators. Each gear stage has torque losses due to Coulomb, viscous, and meshing friction, included in the dynamic model of the leg using the friction model proposed in [7], which is:

$$\tau_{F_i} = [\tau_C + (\tau_E - \tau_C)e^{-|\dot{\theta}_{m_i}|/\dot{\theta}_S} + A_1 sin(\omega_1 \theta_{m_i} + \phi_1) + A_2 e^{-\beta|\dot{\theta}_{m_i}|} sin(\omega_2 \theta_{m_i} + \phi_2)] sign(\dot{\theta}_{m_i}) \quad (16)$$

where subindex i denotes the joint number. This friction model includes a static-friction value, τ_E, a Coulomb-friction value, τ_C, a Stribeck effect, represented by the Stribeck velocity, $\dot{\theta}_S$, a position-dependent friction of amplitude A_1 and frequency ω_1, and a meshing-friction component of variable amplitude and frequency ω_2. The viscous friction in the transmission, F_{vi}, has been included in the equivalent damping term of the actuator. These friction parameters have been identified for the SILO4 leg and are shown in Tables II to IV. Parameter identification has been carried out by th least square method, and it is detailed in [7]. Then let us name the rotor inertia and damping for joint i J_{mi} and B_{mi} respectively, and let us also name the inertia and damping of the elastic coupling element between the planetary gear and the skew-axis gear J_{ei} and B_{ei} respectively. The torque balance of expression (13) for the three joint-motor assemblies of the leg is as follows:

$$\tau_{m1} - \tau_{p1} - \tau_{F1} = (J_{m1} + N_{p1}^{-2} h)\ddot{\theta}_{m1} + (B_{m1} + F_{v1})\dot{\theta}_{m1} \quad (17)$$

$$\tau_{m2} - \tau_{p2} - \tau_{F2} = (J_{m2} + N_{p2}^{-2} J_{e2} + N_{p2}^{-2} N_{s2}^{-2} l)\ddot{\theta}_{m2} + (B_{m2} + N_{p2}^{-2} B_{e2} + F_{v2})\dot{\theta}_{m2} \quad (18)$$

$$\tau_{m3} - \tau_{p3} - \tau_{F3} = (J_{m3} + N_{p3}^{-2} J_{e3} + N_{p3}^{-2} N_{s3}^{-2} m)\ddot{\theta}_{m3} + (B_{m3} + N_{p3}^{-2} B_{e3} + F_{v3})\dot{\theta}_{m3} \quad (19)$$

Actuator dynamic parameters are listed in Table V. Perturbation torques τ_{p1}, τ_{p2}, and τ_{p3} are the torques required in joints 1, 2, and 3 of the leg respectively to follow a given trajectory and are obtained from (12):

$$\tau_{\mathbf{p}} = \mathbf{N}^{-1}\mathbf{D}_2(\theta_m)\mathbf{N}^{-1}\ddot{\theta}_{\mathbf{m}} + \mathbf{N}^{-1}\mathbf{H}(\theta_m, \dot{\theta}_m) + \mathbf{N}^{-1}\mathbf{C}(\theta_m) + \mathbf{N}^{-1}\mathbf{J}^T\mathbf{F} \quad (20)$$

where

$$\tau_{\mathbf{p}} = (\tau_{p1}\ \tau_{p2}\ \tau_{p3})^T \quad (21)$$

$$\mathbf{N} = \begin{pmatrix} N_{p1} & 0 & 0 \\ 0 & N_{p2}N_{s2} & 0 \\ 0 & 0 & N_{p3}N_{s3} \end{pmatrix} \quad (22)$$

Matrices $\mathbf{D_1}$, $\mathbf{D_2}$, $\mathbf{H}$, and $\mathbf{C}$ can be found in Appendix B. Kinematic parameters and the jacobian $\mathbf{J}$ are shown in Appendix A.

4.3. Model analysis

Once the mathematical model of the SILO4 leg has been obtained, the model is analyzed. First, a prototype of the SILO4 leg (shown in Figure 4) is used to analyze the torque contributions of the mechanical part during real leg trajectories, and later the torque contributions of the actuator dynamics are compared. It is well known that accurate and efficient model analysis requires the chosen trajectories to be sufficiently exciting. The trajectories chosen for the analysis of the SILO4-leg model are bang-bang in acceleration to provide sufficiently dynamic excitement. The algorithm used for generation of such optimal trajectories is explained in detail in [6]. Then the experiments are carried out to obtain the torque contributions of the mechanical part of the leg and its actuators while each joint is PID controlled.

4.3.1. *Torque contribution of the mechanical part*

To analyze the dynamics of the mechanical part of the leg, the torque contributions of each term in the mathematical model are compared during real leg-transfer trajectories. Figure 5 shows the torque contributions corresponding to the four terms in the model of

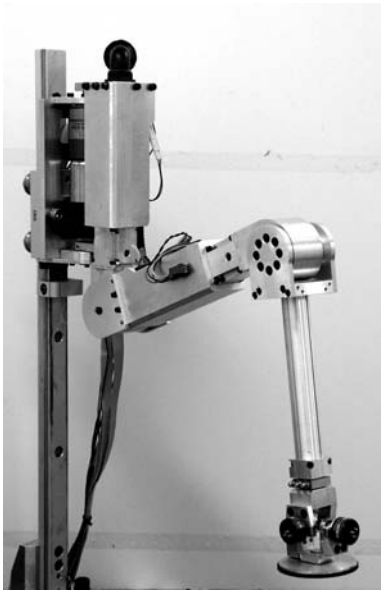

Figure 4. Prototype of the SILO4 leg used for the experiments.

the mechanical part, which are:

$$\begin{aligned} \tau_{\mathbf{D1}} &= \mathbf{D_1}(\mathbf{q})\ddot{\mathbf{q}} \\ \tau_{\mathbf{D2}} &= \mathbf{D_2}(\mathbf{q})\ddot{\mathbf{q}} \\ \tau_{\mathbf{H}} &= \mathbf{H}(\mathbf{q}, \dot{\mathbf{q}}) \\ \tau_{\mathbf{C}} &= \mathbf{C}(\mathbf{q}) \end{aligned} \tag{23}$$

where the total torque contribution of the mechanical part of the leg is:

$$\tau_{\mathbf{e}} = \tau_{\mathbf{D1}} + \tau_{\mathbf{D2}} + \tau_{\mathbf{H}} + \tau_{\mathbf{C}} \tag{24}$$

The terms that contribute to the perturbation torque, τ_p, are:

$$\tau_{\mathbf{p}} = \tau_{\mathbf{D2}} + \tau_{\mathbf{H}} + \tau_{\mathbf{C}} \tag{25}$$

and the term $\tau_{\mathbf{D1}}$ contributes to the actuator equivalent inertia. The time evolution of the torque contribution of this term along a given leg trajectory is represented in Figure 5(a), where each line shows the torque required in each joint to move the constant inertia of its own link (vector τ_{D_1}). Likewise, Figure 5(b) shows the time evolution of the torque contribution of non-constant and non-diagonal inertia terms (vector τ_{D_2}), Figure 5(c) shows the torque contribution of Coriolis

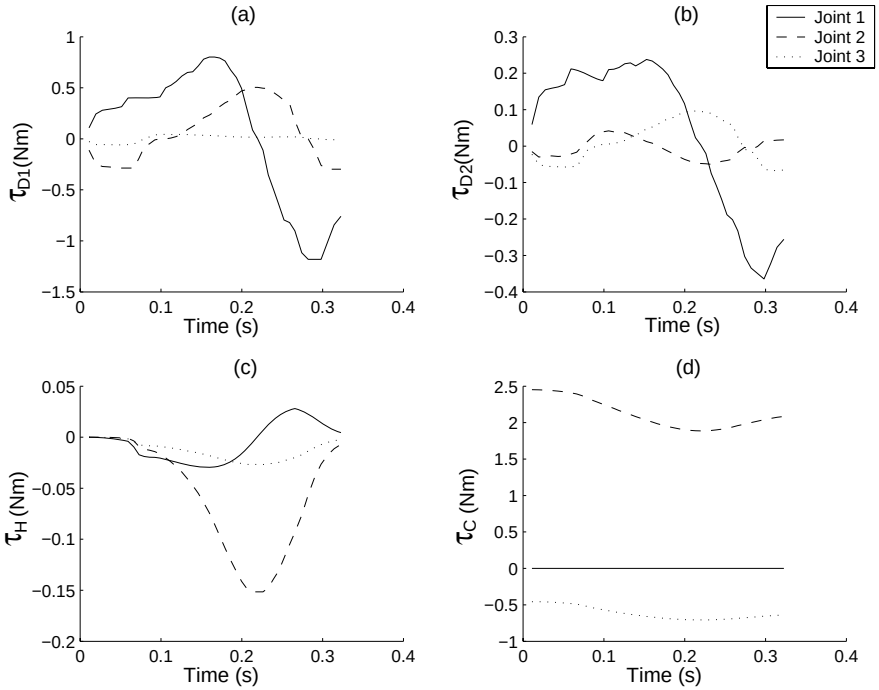

Figure 5. Torque contributions of the mechanical part of the SILO4 leg.

and centrifugal effects (vector τ_H), and Figure 5(d) shows the torque contribution of gravitational effects (vector τ_C).

Detailed numerical comparison of the contributions of the four terms in the dynamic model shows that Coriolis and centrifugal effects play a very little role in leg dynamics (see Figure 5(c)). This can be observed more clearly in Figure 6, where all the torque contributions have been plotted together. Now it is clear that $\tau_{\mathbf{H}}$ can be neglected. The significance of gravitational terms in the motion of joints 2 and 3 is visible, as well as the relevance of constant inertia in joint 1. Figure 7 shows the total perturbation torque of each joint τ_{p_i} in equation (25) and compares it with the simplified perturbation torque obtained by extracting $\tau_{\mathbf{H}}$ from (25), that is:

$$\tau_{\mathbf{p}}^{\mathbf{s}} = \tau_{\mathbf{D2}} + \tau_{\mathbf{C}} \tag{26}$$

Figure 7 also shows the maximum error made in the simplification, which is 4.2% in the worst case.

To conclude the analysis of the mechanical part of the leg, we state that the relevant dynamics affecting the first joint of the SILO4 leg

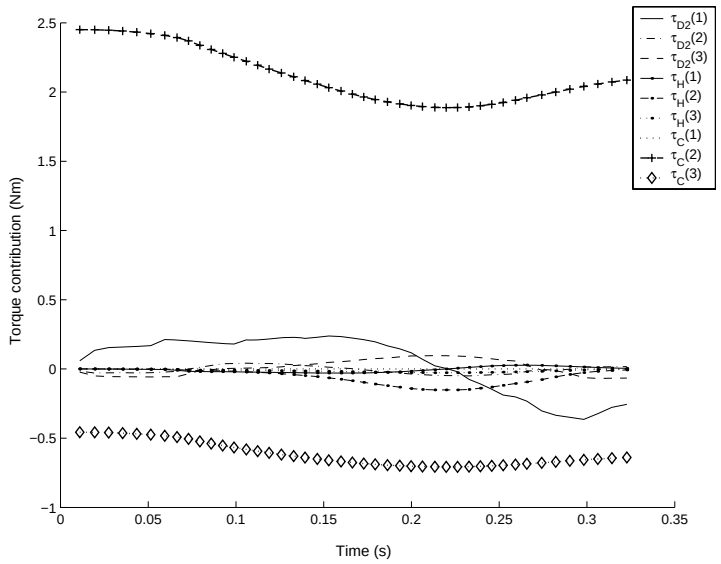

Figure 6. Numerical comparison of torque contributions of the mechanical part of the SILO4 leg.

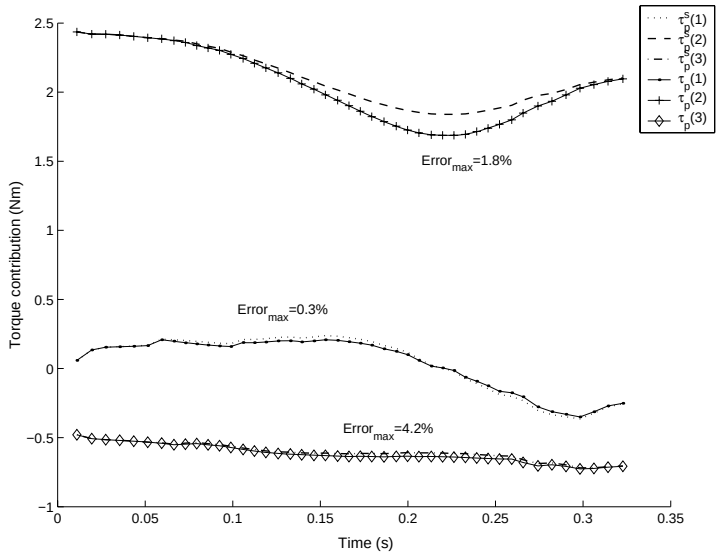

Figure 7. Perturbation torque (τ_p) and simplified perturbation torque (τ_p^s) for the dynamic model of the SILO4 leg.

are inertias, while the dynamics that mainly affect joints 2 and 3 are gravitational effects. Inertias play a secondary role in these two joints.

4.3.2. *Torque contribution of actuators and transmission systems*
Figures 8(a) and (b) show torque contributions due to actuator equivalent inertia and friction, respectively, during a given leg trajectory. Actuator equivalent inertia includes the effect of constant inertia of the mechanical part of the leg, $\mathbf{D_1}$, as in equations (17) to (19). The friction torque has been computed using (16) during real leg trajectories. The comparison of the two figures allows us to state that friction in joints 2 and 3 is twice the inertial contribution. In the first joint, however, inertia is more relevant than friction, yet in any case friction is never negligible. Therefore, the initial guess that friction in high-geared robotic systems is relevant enough to hamper model simplification is here verified. In fact, friction dominates the dynamics of actuators 2 and 3. Therefore, simplification of the dynamic model of walking robots assuming that no friction exists will surely yield significant errors during motion control.

Figure 9 is intended to show the perturbing effect of the mechanical part of the leg on actuator dynamics. For the example trajectory, this perturbation, $\tau_{\mathbf{p}}$, can be considered as constant for actuators 2 and 3. However, the perturbation in actuator 1 is not constant, due to the variable inertia $\mathbf{D_2}$, although it is almost negligible. Figure 10(a) shows the maximum error of neglecting the perturbation in actuator 1 relative to the inertial torque in the actuator for different leg trajectories. The figure shows that this error is always less than 0.5%.

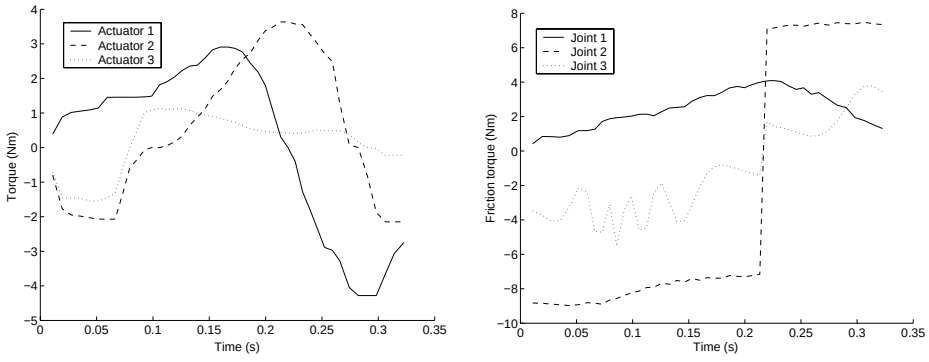

(a) (b)

Figure 8. (a) Torque contribution of actuator equivalent inertia. (b) Torque contribution of friction in actuator-transmission system.

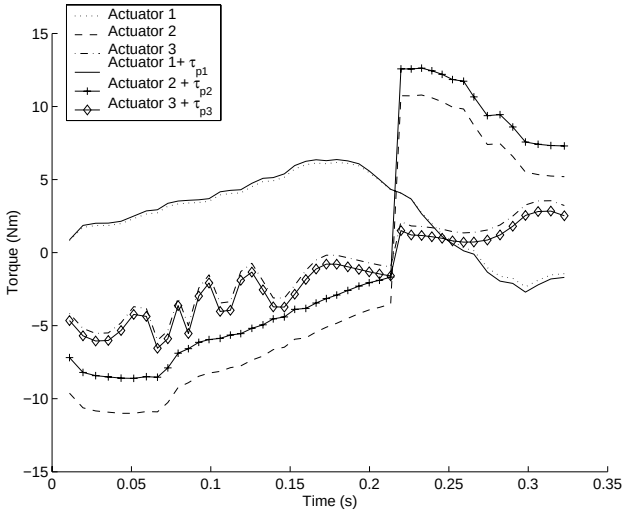

Figure 9. Torque contribution of the actuator model and effect of the perturbation due to the mechanical part of the SILO4 leg.

Let us define the **horizontal lengthening of the leg,** R_h, as the horizontal projection of the distance from the end-effector to the origin of the leg reference frame (see Figure 11). For the SILO4 leg this becomes:

$$R_h = a_3\, cos(q_2 + q_3) + a_2\, cos(q_2) \tag{27}$$

The dominant perturbation of the dynamics of joints 2 and 3 is due to gravity, and this effect increases as the leg stretches horizontally, as shown in Figures 10(b) and 10(c). Also the mathematical dependence of these terms on joint position, q_2 and q_3, is shown in Appendix B.

This analysis of the dynamic model of the SILO4 leg concludes that the effect of the dynamics of the mechanical part on the first joint can be neglected. On the other hand, the perturbation of the mechanical part on joints 2 and 3 varies with the horizontal lengthening of the leg. Based on this consideration, the model can be simplified without losing accuracy. Then the simplified perturbation torques on the three actuators due to the mechanical part of the leg, τ^s_{p1}, τ^s_{p2}, and τ^s_{p3}, are given by:

$$\tau^s_{p1} = 0 \tag{28}$$

$$\tau^s_{p2} = m_2 R_h(q_2, q_3) + b_2 \tag{29}$$

$$\tau^s_{p3} = m_3 R_h(q_2, q_3) + b_3 \tag{30}$$

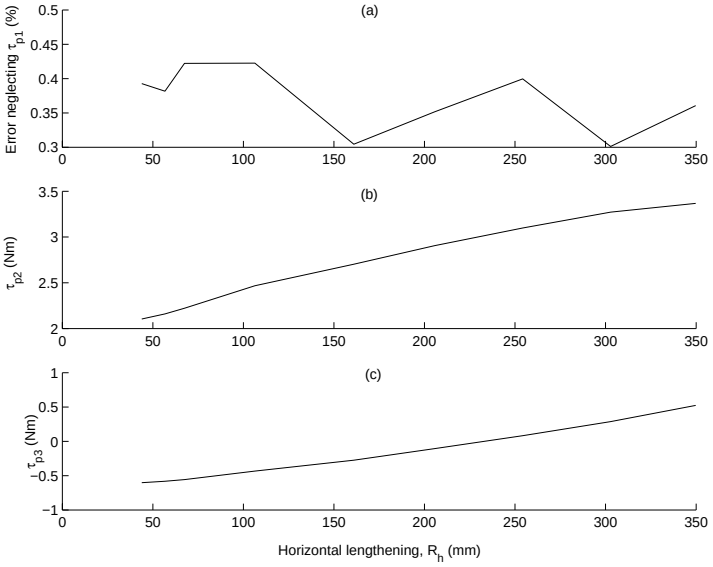

Figure 10. Perturbation torques due to the mechanical part of the SILO4 leg for trajectories of different horizontal length. (a) Maximum error when neglecting τ_{p1}. (b) Evolution of τ_{p2} when increasing the horizontal lengthening. (c) Evolution of τ_{p3} when increasing the horizontal lengthening.

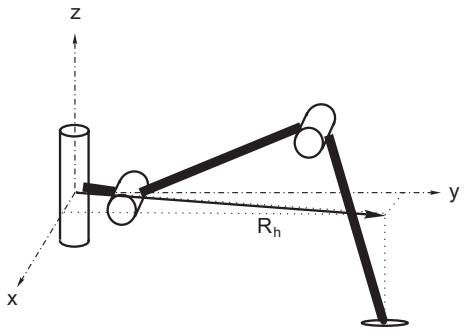

Figure 11. Horizontal lengthening of a robot leg.

where the relationships between τ_{p2}^s, τ_{p3}^s, and R_h have been linearized.

4.4. Real-time control scheme

Our analysis of the dynamic model of the SILO4 leg has produced a simplified model where joints 2 and 3 are coupled while joint 1 is independent. This analysis enables a control strategy based on the computed model. The control algorithm uses the simplified model

to compute the perturbation torque and then compensates for it. Likewise, the friction torque and actuator inertia are pre-computed and compensated for. Figures 12(a) to 12(c) show the control scheme, where each block diagram represents one joint-control flow. The controller of joint i is represented by a transfer function $R_i(s)$, and the relationship between torque and voltage in a DC-motor model has been linearized for the sake of clarity, K_i being the proportionality constant. The non-linear coupling between the control scheme of joints 2 and 3 is solved by means of gain scheduling, where equations (29) and (30) are computed based on joint positions. Controller gains are then tuned for each trajectory.

5. Conclusions

Many authors recommend not taking leg dynamics into account in the control of walking robots. The high gearing employed is often the reason for neglecting the effect of leg dynamics on trajectory control. However, the use of a gear reduction high enough to ignore leg dynamics implies a significant increase in backlash, friction and elasticity in the transmission system. These undesired additional effects are much more difficult to model than the dynamics of the mechanical part. One main conclusion of this paper is that considering robot legs as massless systems is not always the best option. The effect of leg dynamics can be appreciable, and moreover it can be used to improve the control system. In this paper we have derived a precise, accurate model of a robotic leg. Experiments have been done using a real leg prototype to analyze the torque contributions of different dynamic components during real leg trajectories. Detailed analysis of leg dynamics has led us to a simplified, accurate model of the dynamic effect of the leg on motion control. It also enables a controller employed for the dynamic control of this leg to be tuned during trajectory following. The next step in the near future is the real-time control of the SILO4 robot using the leg's dynamic model that we have presented here.

Acknowledgements

This work has been partially funded by CICYT through Grant DPI2001-1595. The CAM sponsored a scholarship granted to the first author for this work.

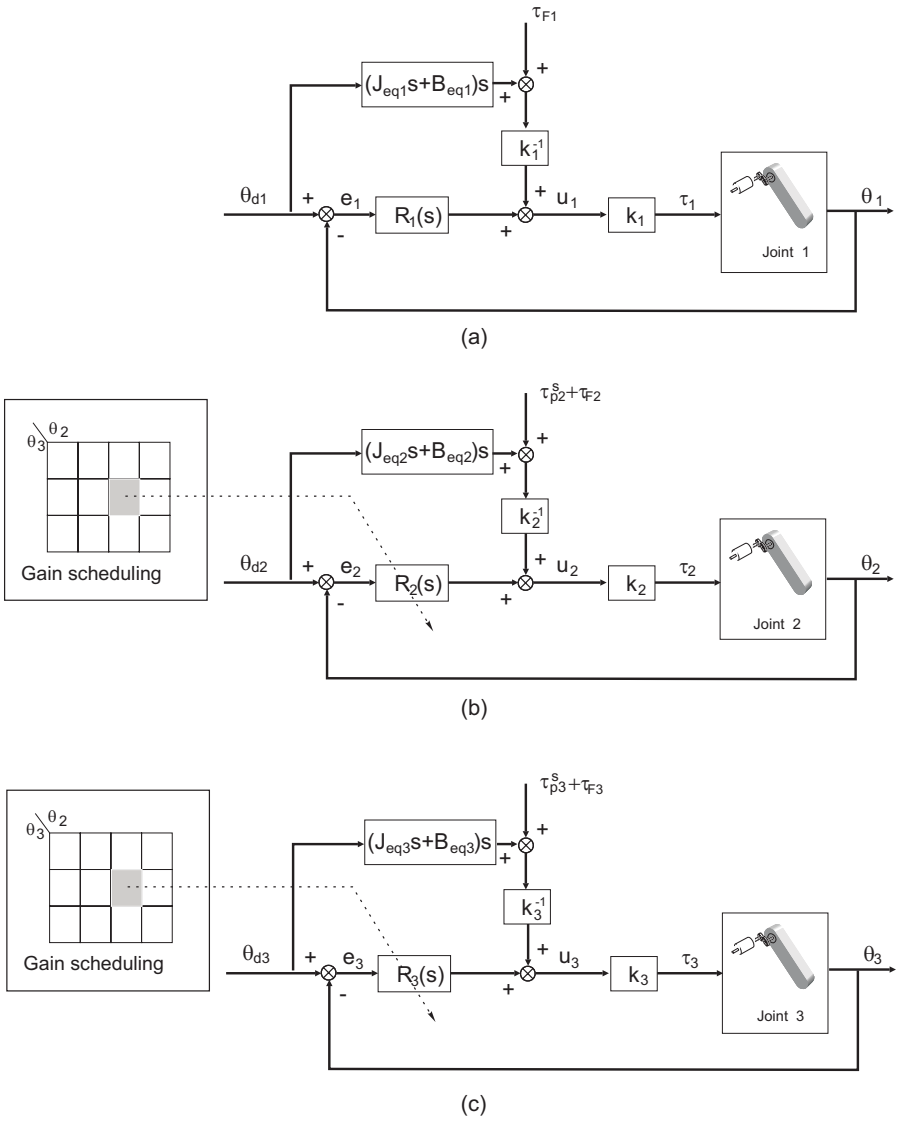

Figure 12. Block diagram of the leg control system. (a) Joint 1. (b) Joint 2. (c) Joint 3.

References

1. Armstrong, B.: 1989, 'On finding excitation trajectories for identification experiments involving systems with nonlinear dynamics'. *The International Journal of Robotic Research* **8**(6), 28–48.

2. Bennani, M. and F. Giri: 1996, 'Dynamic modelling of a four-legged robot'. *Journal of Intelligent and Robotic Systems* **17**, 419–428.
3. Craig, J. J.: 1989, *Introduction to Robotics*. Addison-Wesley, 2nd edition.
4. Dettman, J.: 1988, *Mathematical methods in physics and engineering*. New York: Dover Publications Inc.
5. Fu, K. S., R. C. Gonzalez, and C. S. G. Lee: 1987, *Robotics*. McGraw Hill.
6. Garcia, E. and P. Gonzalez de Santos: 2001, 'Using soft computing techniques for improving foot trajectories in walking machines'. *Journal of Robotic Systems* **18**(7), 343–356.
7. Garcia, E., P. Gonzalez de Santos, and C. Canudas de Wit: 2002, 'Velocity dependence in the cyclic friction arising with gears'. *The International Journal of Robotic Research* **21**(9), 761–771.
8. Lamit, L. G.: 2001, *Pro/ENGINEER 2000i2*. BROOKS/COLE, Thomson Learning.
9. Manko, D.: 1992, *A general model of legged locomotion on natural terrain*. Boston-London-Dordrecht: Kluwer Academic Publishers.
10. Mayeda, H., K. Osuka, and A. Kangawa: 1984, 'A new identification method for serial manipulator arms'. In: *IFAC 9th World Congress*, Vol. 6. pp. 74–79. Budapest.
11. Monagan, M., K. Geddes, G. Labahn, and S. Vorkoetter: 1998, 'MapleV Programming Guide'. Maple Waterloo Software.
12. Ogata, K.: 1996, *Modern Control Engineering*. Prentice Hall, 3rd edition.
13. Pfeiffer, F. and T. Rossmann: 2000, 'About friction in walking machines'. In: *Proc. IEEE Int. Conf. Robotics and Automation*. pp. 2165–2172. San Francisco, CA.
14. Pfeiffer, F. and H. J. Weidemann: 1991, 'Dynamics of the walking stick insect'. *IEEE Control Systems Magazine* **11**(2), 9–13.
15. Sciavicco, L. and B. siciliano: 2000, *Modelling and control of robot manipulators*. London: Springer-Verlag, 2nd edition.
16. Shing, T. K.: 1994, 'Dynamics and Control of Geared Servomechanisms with Backlash and Friction Consideration'. Ph.D. thesis, The University of Maryland.
17. Spong, M. W.: 1987, 'Modeling and control of elastic joint robots'. *ASME Journal of Dynamic Systems, Measurement, and Control* **109**, 310–319.
18. Swevers, J., C. Ganseman, X. Chenut, and J. Samin: 2000, 'Experimental identification of robot dynamics for control'. In: *Proc. IEEE Int. Conf. Robotics and Automation*. pp. 241–246. San Francisco, CA.
19. Zhou, D., K. Low, and T. Zielinska: 2000, 'A stability analysis of walking robots based on leg-end supporting moments'. In: *Proc. IEEE Int. Conf. Robotics and Automation*. pp. 2834–2839. San Francisco, CA.

Appendix

A. Kinematics of the SILO4 leg

The Lagrange-Euler formulation has been used to derive the dynamic model of the SILO4 leg. The Denavit-Hartenberg homogeneous matrix representation has been used to describe the spatial displacement

between neighboring link coordinate frames to obtain the kinematic information. The relevant Denavit-Hartenberg parameters are given in Table VI. They are obtained from the kinematic parameters of the leg, which can be obtained from Figure 13. Finally, the Denavit-Hartenberg homogeneous matrices that contribute to the dynamic model are given in equations (31) to (33). Note that $S_i = sin(q_i)$, $C_i = cos(q_i)$.

$$ {}^0A_1 = \begin{pmatrix} C_1 & 0 & S_1 & a_1C_1 \\ S_1 & 0 & -C_1 & a_1S_1 \\ 0 & 1 & 0 & 0 \\ 0 & 0 & 0 & 1 \end{pmatrix} \tag{31} $$

$$ {}^1A_2 = \begin{pmatrix} C_2 & -S_2 & 0 & a_2C_2 \\ S_2 & C_2 & 0 & a_2S_2 \\ 0 & 0 & 1 & 0 \\ 0 & 0 & 0 & 1 \end{pmatrix} \tag{32} $$

$$ {}^2A_3 = \begin{pmatrix} C_3 & -S_3 & 0 & a_3C_3 \\ S_3 & C_3 & 0 & a_3S_3 \\ 0 & 0 & 1 & 0 \\ 0 & 0 & 0 & 1 \end{pmatrix} \tag{33} $$

The jacobian, that states the relationship between joint speeds and foot speed is given by:

$$ \mathbf{J} = \begin{pmatrix} -S_1(a_3C_{23} + a_2C_2 + a_1 & -C_1(a_3S_{23} + a_2S_2) & -a_3C_1S_{23} \\ C_1(a_3C_{23} + a_2C_2 + a_1 & -S_1(a_3S_{23} + a_2S_2) & -a_3S_1S_{23} \\ 0 & a_3C_{23} + a_2C_2 & a_3C_{23} \end{pmatrix} \tag{34} $$

B. Dynamic model of the SILO4 leg

In this appendix we present the results obtained after applying the Lagrange-Euler formulation to derive the dynamic model of the mechanical part of the SILO4 leg (See equation (2)). Numerical simplifications of the three matrices for the dynamic model of the SILO4 leg have been performed and presented below.

B.1. Mass matrix for the SILO4 leg (D)

The mass matrix is a 3×3 diagonal matrix containing inertia forces between two links of the leg. The general form of this matrix is:

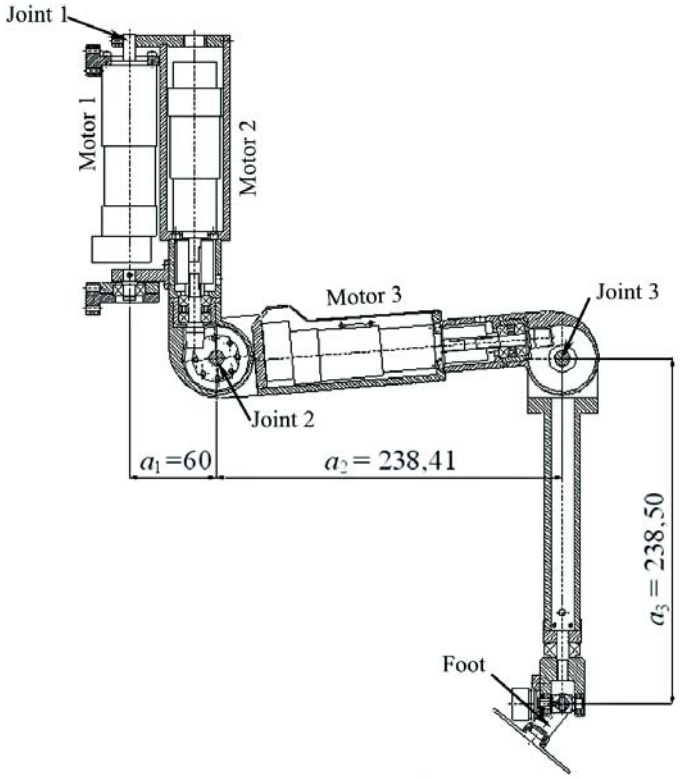

Figure 13. General view of the SILO4 leg.

$$\mathbf{D} = \begin{pmatrix} D_{11} & D_{12} & D_{13} \\ D_{21} & D_{22} & D_{23} \\ D_{31} & D_{32} & D_{33} \end{pmatrix} \tag{35}$$

The contribution of every term of each element of this matrix has been analyzed for different foot trajectories, and finally non-significant terms, whose contribution is less than 10^{-4}, have been omitted. Thus, after these mathematical simplifications, each element of the mass matrix has the following final form:

$$
\begin{aligned}
D_{11} &= aC_2 + bS_2 + cC_3 + dC_{23} + c\,cos(q_3 + 2q_2) \\
&\quad + e\,sin(2q_2) + f\,cos(2q_2) + g\,cos(2q_3 + 2q_2) + h \\
D_{12} &= 0 \\
D_{13} &= 0 \\
D_{22} &= kC_3 + l \\
D_{23} &= cC_3 + m \\
D_{33} &= m
\end{aligned} \tag{36}
$$

where $S_i = sen(q_i)$, $C_i = cos(q_i)$, $S_{ij} = sen(q_i + q_j)$, and $C_{ij} = cos(q_i + q_j)$. The constant and diagonal matrix $\mathbf{D_1}$, whose elements are the constant terms of the diagonal of matrix $\mathbf{D}$, is of the form:

$$
\mathbf{D_1} = \begin{pmatrix} h & 0 & 0 \\ 0 & l & 0 \\ 0 & 0 & m \end{pmatrix} \tag{37}
$$

Constants a to m are listed in Table VII.

B.2. Vector of centrifugal and Coriolis terms (H)

The vector of centrifugal and Coriolis terms is of the form:

$$
\mathbf{H} = (h_1\ h_2\ h_3)^T \tag{38}
$$

where, after analysis and simplification, each element results:

$$
\begin{aligned}
h_1 &= h_{112}\dot{q}_1\dot{q}_2 + h_{113}\dot{q}_1\dot{q}_3 \\
h_2 &= h_{211}\dot{q}_1^2 + h_{223}\dot{q}_2\dot{q}_3 + h_{233}\dot{q}_3^2 \\
h3 &= h_{311}\dot{q}_1^2 + h_{322}\dot{q}_2^2
\end{aligned} \tag{39}
$$

where

$$
\begin{aligned}
h_{112} &= -aS_2 + n\,sen(2q_2) - g\,cos(2q_2) \\
&\quad - dS_{23} - k\,sen(2q_2 + q_3) + p\,sen(2q_2 + 2q_3) \\
h_{113} &= -cS_3 - dS_{23} - c\,sen(2q_2 + q_3) + psen(2q_2 + 2q_3) \\
h_{211} &= qS_2 + f\,sen(2q_2) + r\,cos(2q_2) \\
&\quad + sS_{23} + c\,sen(2q_2 + q_3) + g\,sen(2q_2 + 2q_3) \\
h_{223} &= -kS_3 \\
h_{233} &= -cS_3 \\
h_{311} &= tS_3 + sS_{23} + t\,sen(2q_2 + q_3) + g\,sen(2q_2 + 2q_3) \\
h_{322} &= cS_3
\end{aligned} \tag{40}
$$

Constants a to t are listed in Table VII.

B.3. Vector of gravity terms (G)

The vector of gravity terms is of the form:

$$C = (g_1 \ g_2 \ g_3)^T \tag{41}$$

where, after numerical simplification:

$$\begin{aligned} g_1 &= 0 \\ g_2 &= uC_2 + vS_2 + wC_{23} \\ g_3 &= wC_{23} + xS_{23} \end{aligned} \tag{42}$$

Constants u to x are listed in Table VII.

Table II. Friction parameters identified in the first joint of the SILO4 leg.

Rotation	τ_E (mNm)	τ_C (mNm)	$\dot{\theta}_S$ (rpm-motor)	F_v (mNm/rpm)
Positive	3.019	2.97	38.4	0.00264
Negative	3.019	2.97	38.4	0.00264
	A_1 (mNm)	ω_1 (rad/s)	ϕ_1 (rad)	
Positive	0	$3.5 \cdot 10^{-3}$	0	
Negative	0	$3.5 \cdot 10^{-3}$	0	
	A_2 (mNm)	β_2 (rpm^{-1})	ω_2 (rad/s)	ϕ_2 (rad)
Positive	0.21	$6.5 \cdot 10^{-8}$	1	0.03
Negative	0.23	$5.7 \cdot 10^{-8}$	1	0.03

Table III. Friction parameters identified in the second joint of the SILO4 leg.

Rotation	τ_E (mNm)	τ_C (mNm)	$\dot{\theta}_S$ (rpm-motor)	F_v (mNm/rpm)
Positive	34.91	34.48	5691	0.00123
Negative	34.99	34.53	5702	0.00086
	A_1 (mNm)	ω_1 (rad/s)	ϕ_1 (rad)	
Positive	2.50	$3.5 \cdot 10^{-3}$	0.2	
Negative	2.50	$3.5 \cdot 10^{-3}$	0.2	
	A_2 (mNm)	β_2 (rpm^{-1})	ω_2 (rad/s)	ϕ_2 (rad)
Positive	1.02	$3.1 \cdot 10^{-11}$	0.071	1.2
Negative	1.4	$1.2 \cdot 10^{-11}$	0.071	1.2
	A_3 (mNm)	β_3 (rpm^{-1})	ω_3 (rad/s)	ϕ_3 (rad)
Positive	0.25	$5.8 \cdot 10^{-15}$	1	$-\pi/3$
Negative	0.23	$9.0 \cdot 10^{-16}$	1	$-\pi/3$

Table IV. Friction parameters identified in the third joint of the SILO4 leg.

Rotation	τ_E (mNm)	τ_C (mNm)	$\dot{\theta}_S$ (rpm-motor)	F_v (mNm/rpm)
Positive	8.58	7.106	28.18	0.0134
Negative	9.41	7.909	26.58	0.0138
	A_1 (mNm)	ω_1 (rad/s)	ϕ_1 (rad)	
Positive	0.3	$3.5 \cdot 10^{-3}$	$\pi/2$	
Negative	0.3	$3.5 \cdot 10^{-3}$	$\pi/2$	
	A_2 (mNm)	β_2 (rpm^{-1})	ω_2 (rad/s)	ϕ_2 (rad)
Positive	0.576	$1.27 \cdot 10^{-4}$	0.071	$\pi/2$
Negative	0.526	$1.12 \cdot 10^{-4}$	0.071	$\pi/2$
	A_3 (mNm)	β_3 (rpm^{-1})	ω_3 (rad/s)	ϕ_3 (rad)
Positive	0.133	$5.28 \cdot 10^{-5}$	1	π
Negative	0.152	$7.49 \cdot 10^{-6}$	1	π

Table V. Actuator parameters.

		Actuator 1	Actuator 2	Actuator 3
J_m (10^{-6} Kg m^2)		2.3	6.4	4.9
B_m (10^{-4} Nm/rad/s)		1.77	9.14	3.0
R (Ω)		10.5	2.0	5.5
L (10^{-3} H)		0.94	0.27	0.85
K_M (10^{-3} Nm/A)		46.81	42.88	41.05
K_E (V/rad/s)		0.039	0.043	0.041
Planetary gear	N_p	246	14	14
	η_p (%)	60	80	80
Skew-axis gear	N_s		20.5	20.5
	η_s (%)		70	70
B_e			0.0	0.0
J_e (10^{-6} Kg m^2)			6.5	6.5

Table VI. Denavit-Hartenberg link parameters of the SILO4 leg.

link	$\mathbf{a_i}$	$\mathbf{d_i}$	α_i	θ_i
1	a_1	0	$\pi/2$	θ_1
2	a_2	0	0	θ_2
3	a_3	0	0	θ_3

Table VII. Constant values in SI units for the dynamic model of the SILO4 leg.

a	0.0376	h	0.0532	r	0.00527
b	-0.00173	k	0.0462	s	0.00581
c	0.0231	l	0.0856	t	0.0115
d	0.0116	m	0.0213	u	3.077
e	-0.00528	n	-0.0635	v	-0.142
f	0.0317	p	-0.0210	w	0.951
g	0.0105	q	0.0188	x	0.0152

List of Figures

List of Tables